Graphene from Sugar and its Application in Water Purification

Soujit Sen Gupta,[†] Theruvakkattil Sreenivasan Sreeprasad,[†] Shihabudheen Mundampra Maliyekkal,[‡] Sarit Kumar Das,[§] and Thalappil Pradeep[†,*]
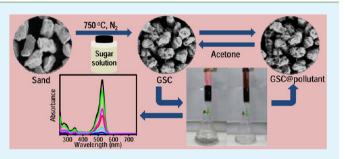
[†]DST Unit on Nanoscience, Department of Chemistry, Indian Institute of Technology Madras, Chennai 600 036, India
[‡]School of Mechanical and Building Sciences, VIT University, Chennai Campus, Chennai 600 048, India
[§]Department of Mechanical Engineering, Indian Institute of Technology Madras, Chennai -600036, India

Ⓢ *Supporting Information*

ABSTRACT: This paper describes a green method for the synthesis of graphenic material from cane sugar, a common disaccharide. A suitable methodology was introduced to immobilize this material on sand without the need of any binder, resulting in a composite, referred to as graphene sand composite (GSC). Raman spectroscopy confirmed that the material is indeed graphenic in nature, having G and D bands at 1597 and 1338 cm^{-1}, respectively. It effectively removes contaminants from water. Here, we use rhodamine 6G (R6G) as a model dye and chloropyrifos (CP) as a model pesticide to

demonstrate this application. The spectroscopic and microscopic analyses coupled with adsorption experiments revealed that physical adsorption plays a dominant role in the adsorption process. Isotherm data in batch experiments show an adsorption capacity of 55 mg/g for R6G and 48 mg/g for CP, which are superior to that of activated carbon. The adsorbent can be easily regenerated using a suitable eluent. This quick and cost-effective technique for the into a commercial water filter with appropriate engineering.

KEYWORDS: *graphene, composites, adsorption, water purification, nanotechnology, environmental remediation*

◼ INTRODUCTION

One of the most socially relevant aspects of nanotechnology is in the field of environmental remediation. Diverse applications of nanomaterials in decontamination of air, water and soil are intensely pursued in the recent past.[1] The availability of large surface area and unusual electronic structure imparts new properties to nanomaterials. One of the early applications of such materials is the halocarbon decomposition and the use of this technology in pesticide removal.[2] Numerous other applications of noble metal nanoparticles have been reported in the literature.[3] Chemical interaction at noble metal nanoparticle surfaces often led to charge transfer and subsequent cleavage of chemical bonds, the most often encountered is reductive dehalogenation.[4] Enhanced surface chemistry leading to faster kinetics is reported on noble metal nanoparticles.[5]

Carbon has been the most versatile material used for water purification in history.[6,7] Very early account of the use of charcoal in water purification is found in the *Vedic* literature.[8] It is believed that people of Indus valley civilization used carbon and porous materials, such as earthen vessels, for filtering and storing drinking water. The most widely used material for water purification today is activated carbon (AC)[9−13] derived from plant sources. It has the best possible surface area and could be produced at low cost, making it the most affordable adsorption medium in diverse applications. A number of other forms of carbon have appeared with very large adsorption capacities.[14] Advanced techniques such as membrane filtration, reverse

osmosis and ion-exchange can be used in treatment and removal of contaminants from water.[15,16] However, higher cost limits the large scale application of such treatment techniques in developing countries.

One of the fascinating new additions into the carbon family is graphene,[17] the one-atom thick sheets of carbon. Carbon materials, such as activated carbon,[18] charcoal, carbon nanotubes,[19,20] have been used extensively in water purification[21] and, hence, are indispensible components of all commercial water technologies.[22,23] It is natural to look at the application of graphene in various aspects of environmental remediation. Several aspects, such as high thermal and electrical conductivity, electronic properties, quantum hall effect, and application in drug delivery[24] and DNA sensing,[25,26] have been investigated in the recent past. We and others[27,28] have shown that chemically synthesized graphene, as well as graphene oxide, can be anchored onto the surfaces of river sand to make effective adsorbents that remove heavy metal ions,[29−34] pesticides,[35] and natural dyes.[36−39] Such materials show higher adsorption capacity in comparison to activated carbon when equal masses of carbon are compared. When used as a stationary adsorbent material in a flowing water stream, it is necessary to anchor the nanoscale adsorbent onto inexpensive and reliable substrates.[40,41] This is to

Scheme 1. Upper Frame Shows a Schematic Diagram of the Preparation of Graphene−Sand Composite[a]

[a]Lower frame shows photographs of pristine sand and GSC.

overcome engineering issues like solid−liquid separation and pressure drop.[42,43] There have been other approaches to attach graphene on sand surfaces with the help of suitable binder such as chitosan[28] or by functionalizing the sand surface.[27]

Utilization of such technologies in people-oriented applications requires the materials to be affordable. In this regard, biologically derived carbon is perhaps the most affordable and chemically most versatile. Materials derived from plant sources may even be more eco-friendly than those from fossil source[44] such as petroleum. Among the simplest of natural sources of carbon are sugars,[45] which upon dehydrogenation get converted completely to elemental carbon, leaving only water to escape. For example,

$$C_{12}H_{22}O_{11} \xrightarrow{\Delta} 12C + 11H_2O \qquad (1)$$

Similar reactions are applicable to decomposition of sugars of various kinds. This transformation is simple and effective. The carbon so obtained could be anchored on inorganic surfaces, and a subsequent chemical treatment could transform it to graphenic carbon (GC). Activation of newly formed surfaces may produce highly effective adsorbents.

In this paper, we report in situ creation of graphenic material anchored onto the surfaces of river sand without the need of any additional binder. We also report the application of this material in water purification. The material shows strong adsorption capability. It could completely decolorize, for example, some of the colored commercial soft drinks. The extension of this chemistry to diverse sugars and carbohydrates in general could contribute to the creation of inexpensive and efficient adsorbents.

■ MATERIAL AND METHODS

The raw materials used for the synthesis were common sugar, river sand, and sulfuric acid. River sand (∼0.2 mm particle size) and sugar were obtained from the local market. Sulfuric acid and acetone were procured from local suppliers, rhodamine 6G chloride ($C_{27}H_{29}ClN_2O_3$) and chlorpyrifos (CP) (HPLC assay 99.9%) were from Sigma Aldrich and soft drink (Coca Cola) was from Hindustan coca-cola beverages Pvt. Ltd. No additional purification was done and the solvent generally used was water unless otherwise mentioned.

Instrumentation. UV−vis spectra were recorded using a Perkin-Elmer Lambda 25 spectrophotometer. Raman spectra were collected using a confocal Raman spectrometer (WiTec GmbH CRM 200) with a 532 nm Nd:YAG laser as the light source. XPS measurements were done

with Omicron ESCA Probe spectrometer with unmonochromatized Mg K_α X-rays (hν = 1253.6 eV). Most of the spectra were deconvoluted to their component peaks using the software CasaXPS. The energy resolution of the spectrometer was set at 0.1 eV at a pass energy of 20 eV. Binding energy was corrected with respect to C 1s at 284.5 eV. Surface morphology, elemental analysis, and elemental mapping studies were carried out using a scanning electron microscope (SEM) equipped with an energy dispersive analysis of X-rays (EDAX) facility (FEI Quanta 200, Czechoslovakia). High-resolution transmission electron microscopy (HRTEM) of the samples was carried out using a JEOL 3010 instrument with a UHR pole piece. For mass analyses, an Applied Biosystems Voyager DE Pro LDI MS instrument was used. A pulsed nitrogen laser of 337 nm was used for desorption/ionization.

Preparation of the Composite. Common sugar (sucrose crystals) was used as the carbon source. At first, the sugar was dissolved in water and then, the solution was mixed with requisite amount of sand (river sand). Calculated amounts of sugar and sand were taken to make different loading ratios. In each case, the mixture was dried at ∼95 °C in a hot air oven for about 6 h with constant stirring. The sugar-coated sand was then placed in a silica crucible and heated in a furnace in N_2 atmosphere. The furnace temperature was programmed as follows: (a) from room temperature to 100 °C in 30 min, (b) 100−200 °C in 30 min (c), held at 200 °C for 1 h (to melt sugar to form a uniform coating; melting point of sucrose is around 186 °C), (d) ramped to 750 °C in 1 h, and (e) held for 3 h at 750 °C (to ensure complete graphitization of sugar). The furnace was switched off and the material was cooled to room temperature. The temperature of 750 ± 5 °C was chosen as the final temperature after optimization through several experiments. No special care was taken in controlling the cooling rate. The black sample was named graphene sand composite (GSC). For activation, 5 g of the composite was treated with 10 mL of concentrated sulfuric acid and kept undisturbed at room temperature for 30 min. The mixture was then filtered and dried at 120 °C. The activated GSC is labeled as GSC_{750}. The lower frame of Scheme 1 shows the photographs of sand (before coating) and GSC.

Adsorption Experiments. Time-dependent adsorption capacity of the as-synthesized composite was investigated in a batch reactor of 25 mL capacity. The working volume and the adsorbent dose were maintained as 10 mL and 100 mg, respectively. Water was spiked with the required concentration of rhodamine 6G (R6G) and kept with GSC for stirring at room temperature (30 ± 2 °C). The solid−liquid separation was done by filtration. The filtrate was analyzed for R6G using UV−vis spectrophotometer. The target molecules in the aqueous phase were quantified using the absorbance at 527 nm. All the experiments were conducted in duplicate and the samples were analyzed immediately. Similar experiments were done with CP, which has an absorbance peak at 297 nm.
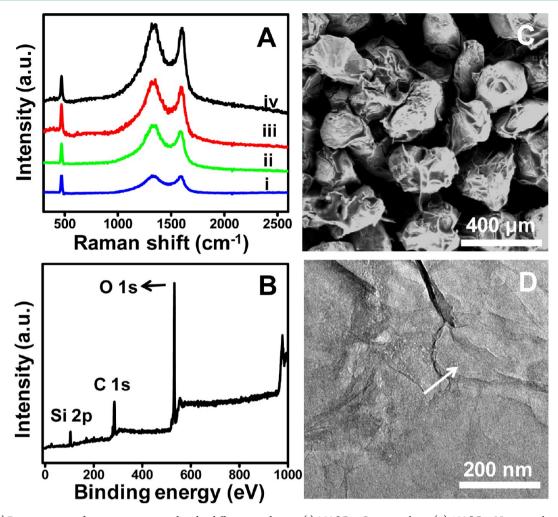
Figure 1. (A) Raman spectra of composites prepared under different conditions: (i) 250 °C in O_2 atmosphere, (ii) 450 °C in N_2 atmosphere, (iii) 600 °C in N_2 atmosphere, (iv) 750 °C in N_2 atmosphere. (B) XPS survey spectrum of GSC. (C) SEM images of graphene sand composite and (D) TEM image of extracted graphenic sheets.

To measure the adsorption capacity, a fixed-bed column was operated under down flow mode at a feed flow rate of 2.19 $cm^3/cm^2/min$ and feed (R6G) concentration of 1 mg/L. The column was made by packing GSC$_{750}$ to different depth in a transparent glass tube with a length of 50 cm and an internal diameter of 8 mm. The performance of the column was evaluated as a function of time at room temperature. Residual concentration of the pollutant in the effluent samples was determined using UV−vis spectrophotometry. Similar column was packed for decolorizing colored matters from soft drinks. The column bed after exhaustion with pollutant was regenerated using acetone as eluent and was reused for three cycles.

RESULTS AND DISCUSSION

The experimental protocol is outlined in Scheme 1. After the sugar solution was dried on sand and slow carbonization at 200 °C, the material was rapidly heated to 750 °C, to ensure complete graphitization. This results in the formation of a strongly adhering char deposit on the sand surface. Washing with concentrated sulphuric acid produces the composite with higher adsorption sites. In Figure 1, we show the Raman spectrum of the 1 wt % GC loaded composite. We see the evolution of D and G bands as a function of carbonization temperature. The increase in peak intensity with increase in temperature suggests that the formation of graphenic material is better at higher temperatures. The occurrence of sharp G band at 1597 cm^{-1} suggests complete graphitization of the material. The D band at 1338 cm^{-1} suggests

the presence of defect sites needed for adsorption. No 2D feature was observed as typical of such chemically synthesized analogues of graphene.[28,45] The optimum temperature is around 750 °C (N_2 atmosphere), where maximum peak intensity is observed. Upon heating the same material at 800 °C, adhesion to the surface becomes poor and the adsorption capacity decreases (see Figure S1A in Supporting Information). The optimum heating time was found to be 6 h. On increasing the heating time beyond 6 h, there was no further improvement in adsorption capacity (Supporting Information: Figure S1B). The peak at 470 cm^{-1} is due to sand (SiO_2) present in the material, validating the name given (GSC). The peak corresponding to silica is completely masked at higher weight percent of carbon loading, as expected. Raman spectra of sand and sugar-coated sand are shown in Figure S2 of the Supporting Information.

The graphenic morphology is evident in the SEM images: thin sheets of carbon are protruding outward, as seen in Figure 1C. Thicknesses of these sheets are in nanometer regime. After sonicating GSC for 2 h in ethanol, the TEM images of the supernatant solution was taken. Now the images show the presence of nanometer-sized thin sheets (Figure 1D). Also seen are a few wrinkles at the edges which are characteristic of graphene-like material.[32,43] An AFM image shows few layered graphenic material (Supporting Information, Figure S3A), the
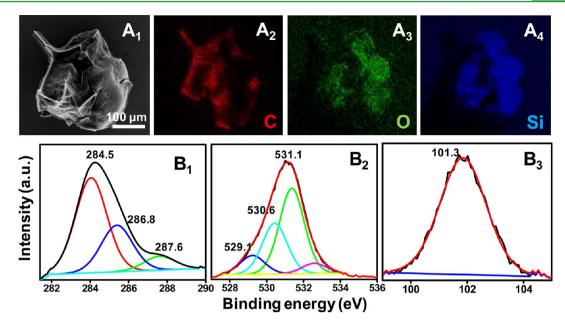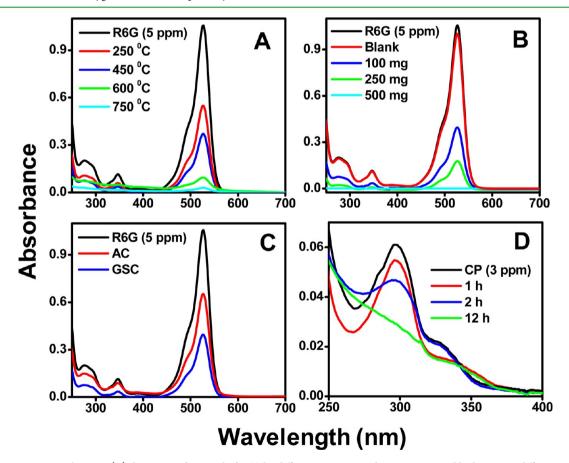
Figure 2. A_1 shows the SEM image of a single GSC particle. A_2. A_3 and A_4 are carbon, oxygen, and silicon maps of GSC. B_1, B_2, and B_3 show the deconvoluted XPS of carbon, oxygen and silicon, respectively.

Figure 3. UV−vis spectra showing, (A) the extent of removal of R6G by different composites that were prepared by heating at different temperatures, (B) removal capacity, when different amounts of GSC_{750} composite were added, (C) comparison of removal capacity among GSC_{750} and AC, and (D) removal capacity of GSC_{750} when CP was used as the contaminant.

height profile shows that the average thickness of the layers is 0.8 nm (Supporting Information, Figure S3B).

The physical appearance of the sand changes completely upon carbon loading (Scheme 1). The deposition of GC and its growth is visible in SEM images. The growth of carbon on SiO_2 surface is evident on the elemental mapping. The elemental maps of GSC (Figure 2, A_1 to A_4) confirm the presence of C, O and Si. XPS is especially useful in understanding the chemical functionality of the material. For GSC, it shows all the expected elements: carbon, oxygen and silicon, as shown in the survey spectrum of
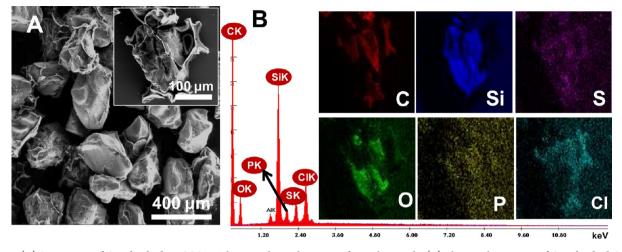
Figure 4. (A) SEM image of CP adsorbed on GSC_{750}. The inset shows the image of a single particle. (B) Elemental mappings of CP-adsorbed GSC_{750}.

the composite (Figure 1B). The existence of various functionalities is evident in the XPS spectrum. Figure 2 (B_1 to B_3) shows the deconvoluted peaks corresponding to carbon, oxygen and silicon in the spectrum. The presence of high percentage of nonoxygenated C 1s (peak centered at 284.5 eV) is a sign of extended carbon backbone. Oxygenated C as C−O (peak at 286.8 eV) is due to the presence of oxygen functionality. The presence of functional oxygen group is responsible for adsorption.[46−48] Deconvolution of the O 1s spectrum gives three components: the first component centered around 531.1 eV, the second around 530.6 eV and the third around 529.1 eV, corresponding to C−O, C=O and O−C=O entities, respectively. The Si 2p peak is weak, as expected in view of the surface coverage. The peak is centered at 101.3 eV, expected for SiO_2. Similar features are observed at varying coverages (Figure S4 of the Supporting Information).
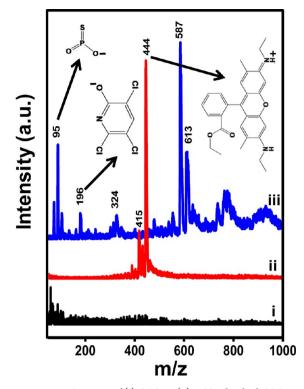
Batch experiment was conducted to assess the adsorption capacity of the material. As discussed earlier, the main focus of this work is effective and economically feasible removal of contaminants present in water. GSC turned out to be an excellent adsorbent for removal of such contaminants. To demonstrate this, we took R6G as the model dye and CP as the model pesticide. Figure 3A shows the removal capacity of composites prepared at different temperatures. Four different preparations were taken: Composites heated at (i) 250 °C in O_2 atmosphere, (ii) 450 °C, (iii) 600 °C, and (iv) 750 °C (all three in N_2 atmospheres). It was noticed that with equal amount of composite (500 mg) and GC loading (1 wt %), the sample prepared at 750 °C in N_2 atmosphere turned out to be the best adsorbent. So, we took this sample for further activation using sulphuric acid treatment to get GSC_{750}. The SEM image and elemental mapping of GSC_{750} are shown in Figure S5 in Supporting Information. Previous studies have reported that the mechanism of dye adsorption on graphene is mainly $\pi−\pi$ interaction.[49] The pollutant-removal capacity of the composite increases after activation. This conclusion was drawn after performing batch experiments with equal amounts of samples to remove R6G (5 ppm) (Figure S6 in Supporting Information). Figure 3B shows the adsorption capacity when different amounts of GSC_{750} were used. It was seen that, for 500 mg, the sample completely removes R6G (5 mg/L) from 10 mL of solution in 2 h. A blank test was performed with river sand (500 mg) alone heated at 750 °C in nitrogen atmosphere which showed negligible removal capacity. Upon quantitative analysis (depicted

in Figure 3C), the adsorption capacity of GSC_{750} for R6G was measured to be 55 mg/g, which is superior to that of activated carbon (32 mg/g). As AC cannot bind to the sand surface by itself, we used chitosan as a binder. The maximum adsorption capacity for R6G for AC was 44.7 mg/g under optimized condition, as found in the literature.[50] Figure 3D shows the removal capacity of GSC_{750}, when CP is used as the contaminant. 100 mg of the composite removes CP (3 ppm) completely from 10 mL of the solution in 12 h. CP has a characteristic absorption peak at 297 nm. The gradual decrease of intensity with time indicates that CP is being removed from water.

Adsorption of pollutant is evident from SEM results. Experiments were conducted with CP. SEM images (Figure 4A) show that the morphology of the substances does not change significantly after adsorption. Inset in Figure 4A shows a single particle on which elemental mapping was performed. From the mappings (Figure 4B), in CP-adsorbed composite, we see the presence of P and Cl, besides those present in original GSC_{750} (shown in Supporting Information in Figure S5). This observation confirms that adsorption on GSC had indeed taken place. The P and Cl images overlap with Si and C images due to GSC_{750}.

The retention of the adsorbed species in the molecular form on the surface of GSC_{750} is supported by laser desorption ionization mass spectrometry (LDI MS). The spectrum suggests the existence of the adsorbate in an integral form. No chemical transformation is observed. There was no prominent peak originating from the GSC_{750}, either in positive or negative mode (Figure 5(i)). In Figure 5(ii), the peak at m/z 444, observed for R6G adsorbed on GSC_{750}, represents the integral molecular ion, $C_{28}H_{31}N_2O_3^+$. The other peak at m/z 415 corresponds to a fragmented product formed during LDI analysis by elimination of an ethyl group from R6G. The spectrum in the negative mode of LDI MS of CP adsorbed on GSC_{750} has some characteristic peak at m/z 196 and 95 corresponding to $C_5HCl_3NO^-$ and $(O_2PS)^-$, respectively. The peak at m/z 324 is the fragmented product due to the elimination of C_2H_4 from the molecular ion peak at m/z 352. The peaks at m/z 587 and 613 are due to some fragmented dimers of CP. The structures of these most common fragments are shown in Figure 5. The XPS analysis of sample after adsorption of R6G is shown in Supporting Information in Figure S7, which shows that nitrogen due to R6G is present on the material. The N 1s features observed around 397.9 and 399.9 eV are due to two different chemical environments, under-
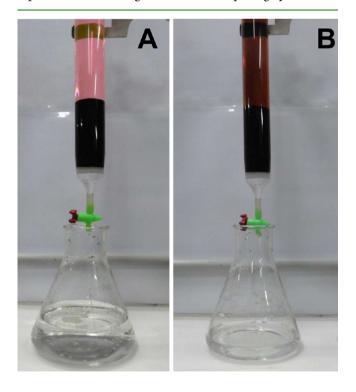
Figure 5. LDI MS spectra of (i) GSC$_{750}$, (ii) R6G-adsorbed GSC$_{750}$, and (iii) CP-adsorbed GSC$_{750}$. The structures of some of the ions detected are shown.

standable from the structure of R6G. The nitrogen peak for R6G adsorbed on GSC$_{750}$ was masked by the intense carbon peak in EDAX.
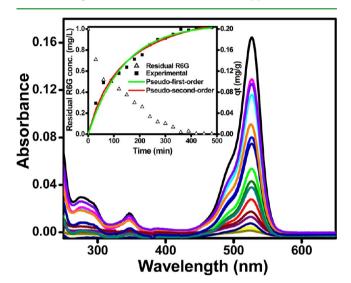
Performance of the material was tested in the column experiment as well. Figure 6 shows the photographs of two

Figure 6. Photographs of adsorption columns using GSC$_{750}$ for separating (A) R6G from an aqueous solution and (B) coca cola.

columns packed with GSC$_{750}$ (1 wt % GC loading). The columns had a diameter of 2 cm and the bed height was 6 cm. Complete removal of the colored matter is evident from decolorization of the filtrate when the column was run with R6G and coca cola. Analysis of mass spectrum of the filtrate was carried out to confirm the presence/absence of R6G. No characteristic peaks of R6G fragments were seen. This observation ensures the complete removal of R6G.

The interaction between R6G and the adsorbent composite was investigated as a function of time using 100 mg of the adsorbent and 10 mL of 1 ppm R6G solution. The data are shown in Figure 7. From the results, it is apparent that the
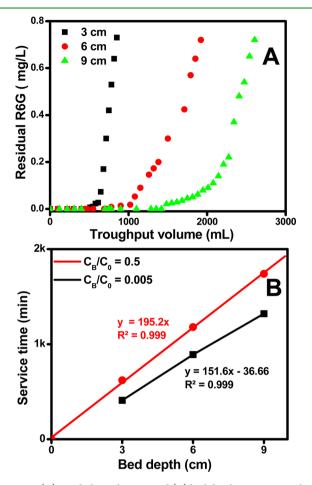

Figure 7. Kinetic study of the adsorption of R6G by GSC$_{750}$ in a batch experiment, time interval was 30 min. Inset shows the pseudofirst and pseudosecond order model fits (secondary axis); the primary axis of the inset figure shows the kinetic data obtained from the experiment.

composite could remove R6G completely in 8 h of contact time starting from the commencement of the adsorption process. During time-dependent study, the characteristic absorption peak at 527 nm corresponding to R6G was monitored. As a function of time, the intensity of the peak for the treated solution initially decreases rapidly and then the change in intensity slows down. This is because of the decreasing number of unoccupied adsorption sites with increasing time. After 8 h, the characteristic peak is absent, which emphasizes the complete removal of R6G from the solution. Thus, the equilibrium time was fixed at 8 h. The kinetic data were described by Lagergren pseudo-first-order[51,52] and Ho's pseudo-second-order kinetic models.[53] The mathematical representations of these models are given elsewhere.[54] A nonlinear method was used to find the best-fitting model and kinetic parameters, which were found by trial and error method by means of Microsoft's spreadsheet, Excel software package using solver add-in option. The plots of model equation along with the experimental data are given in the inset of Figure 7. The suitability of the models to describe the data was examined using the chi square (χ^2) value. Smaller χ^2 value indicates better curve fitting. The analysis showed that a pseudo second-order equation is more appropriate in describing the experimental data.

Continuous Flow Experiments. Continuous flow experiments were conducted as a function of adsorbent bed depth to test the adsorption capacity and service time of the bed in removing R6G from water. The performance of the bed was

evaluated using the breakthrough curves (Figure 8A). The data obtained from the study are summarized in Table 1. As evident

Figure 8. (A) Break through curve and (B) bed depth service time plots for the adsorption of R6G by GSC$_{750}$ in columns.

Table 1. Performance of Columns Packed with Graphene-Sand Composites at Different Bed Depths

bed depth, Z (cm)	empty bed contact time, t_{EB} (min)	breakthrough time, t_B (min)	throughput volume, V_{TB} (mL)	adsorption capacity (mg/g of carbon)
3	1.37	450	860	23.45
6	2.74	960	1950	24.55
9	4.11	1452	2706	26.63

from the figures, adsorption was affected by change in bed depth. Increase in bed depth increases the volume of treated water because of higher contact time and availability of more adsorption sites. At lower bed depths, the curve became steeper showing the quicker exhaustion of the fixed bed. A Bed Depth Service Time model (BDST) model, a successful method of analyzing data from column tests,[55] is generally used for predicting the performance of the adsorbent columns. The model gives a linear relationship between the time required to reach the desired breakthrough concentration (t_B) and the bed depth (Z), represented as

$$t_B = \frac{N_0}{C_0 U_0} Z - \frac{1}{K_{BD} C_0} \ln\left(\frac{C_0}{C_B} - 1\right) \tag{2}$$

Here, N_0 is the saturation concentration per unit volume of bed (mg/L), C_0 is influent solute concentration (mg/L), C_B is the desired concentration of solute at breakthrough (mg/L), U_0 is the linear flow velocity (cm/min), and K_{BD} is the adsorption rate constant L/(mg min).

Figure 8B shows the plots of service time versus bed height for the adsorbent packed in column. From the results, it is clear that variation of service time with bed depth is linear, suggesting that this model is valid for predicting column performance at breakthrough point. The BDST parameters, namely, K_{BD} and N_0, are 144.62 mg/cm^3 and 0.33 cm^3/mg/min, respectively (C_B/Co = 0.005). The corresponding N_0 value for 50% saturation points ($C_B/C_0 = 0.5$) is 0.43 cm^3/mg/min. It is also evident that the calculated adsorption capacity at 50% saturation is greater than that at 0.5% saturation.

Regeneration and Reuse. Any adsorption process is economically more viable if the adsorbent can be regenerated and reused many times. Regeneration study will also give an insight into whether the material after use is safe for disposal or not. The present study focuses on developing a proper regeneration protocol for exhausted composite as well. For this, adsorption study was carried out with the as-synthesized adsorbent using 1 mg/L of R6G solution at neural pH. The R6G-loaded GSC$_{750}$ was regenerated in situ in the columns using acetone as the eluent. The regenerant (acetone) was passed through the column at a flow rate of 1 mL/min. Nearly 30 bed volumes of acetone were passed through the column in down-flow mode. Samples of eluted acetone-R6G solution and the aqueous wash liquid were collected and analyzed for determining the concentrations of R6G as function of time. After complete desorption, the bed was purged with hot air (hair dryer was used for this purpose) to remove residual acetone in the bed. In order to test the feasibility of repeated use of the adsorbent bed, three consecutive adsorption/desorption cycles were performed. For a 3 cm column, the adsorption capacity was 23.45 mg/g (Table 1) for the first run, 22.78 mg/g for the second run and 22.07 mg/g for the third run. Note that the capacity given is from the column data which are generally lower than the equilibrium adsorption capacities derived from batch data. These results indicate that the material could be reused for several cycles without the performance of the material being adversely affected. SEM images of bare sand and the regenerated GSC$_{750}$ after first cycle are given in Supporting Information (Figure S8), which show that the morphology of GSC$_{750}$ does not change after regeneration.

■ CONCLUSION

We have established the synthesis of sugar-derived graphenic material supported on sand. Complete conversion of sugar to graphenic carbon suggests a green methodology for the creation of an active adsorbent material. We used R6G as the model dye and CP as the model pesticide, to show the adsorption capacity of the material. The batch experiment shows an adsorption capacity of 50–55 mg/g for R6G. The best capacity determined for R6G for AC under optimized condition was 44.7 mg/g.[50] The performance validates the use of this material as an active medium for commercial applications. The utilization of this material for water purification is evident from the data presented. The large adsorption capacity, green methodology and the availability of the materials across the world enables it to be used in different parts of the world. Materials of this kind are expected to contribute to developing affordable solutions for drinking water.

■ ASSOCIATED CONTENT

ⓢ Supporting Information

UV–vis spectra pertaining to the optimization of heating time and temperature, Raman spectra of sand and sugar coated sand, AFM image and height profile of the graphenic material, XPS of GSC at different carbon loading, SEM and EDAX of GSC after acid wash, UV–vis spectrum showing GSC after acid wash, XPS analyses of R6G-adsorbed GSC_{750} and SEM image of sand and GSC_{750} after regeneration. This information is available free of charge via the Internet at http://pubs.acs.org/.

■ AUTHOR INFORMATION

Corresponding Author
*E-mail: pradeep@iitm.ac.in. Fax: 91-44-2257-0545/0509.

Notes
The authors declare no competing financial interest.

■ ACKNOWLEDGMENTS

■ REFERENCES

(1) Litter, M. I.; Choi, W.; Dionysiou, D. D.; Falaras, P.; Hiskia, A.; Li Puma, G.; Pradeep, T.; Zhao, J. *J. Hazard. Mater.* **2012**, *211–212*, 1–2.

(2) Pradeep, T.; Anshup. *Thin Solid Films* **2009**, *517*, 6441–6478.

(3) Gupta, R.; Kulkarni, G. U. *ChemSusChem* **2011**, *4*, 737–743.

(4) Matheson, L. J.; Tratnyek, P. G. *Environ. Sci. Technol.* **1994**, *28*, 2045–2053.

(5) Bootharaju, M. S.; Pradeep, T. *Langmuir* **2012**, *28*, 2671–2679.

(6) Zhang, S.; Li, X.-y.; Chen, J. P. *Carbon* **2010**, *48*, 60–67.

(7) Novoselov, K. S.; Geim, A. K.; Morozov, S. V.; Jiang, D.; Zhang, Y.; Dubonos, S. V.; Grigorieva, I. V.; Firsov, A. A. *Science* **2004**, *306*, 666–669.

(8) Anonymous. *Lancet* **1912**, *180*, 1025–1026.

(9) Adams, B. A. *Lancet* **1932**, *219*, 724–724.

(10) Kämpf, H. J. *Water Res.* **1972**, *6*, 493–494.

(11) Goyal, M.; Bhagat, M.; Dhawan, R. *J. Hazard. Mater.* **2009**, *171*, 1009–1015.

(12) Hager, D. G. *Environ. Sci. Technol.* **1967**, *1*, 287–291.

(13) Ghosh, P. K.; Philip, L. *J. Environ. Sci. Health., Part B* **2005**, *40*, 425–441.

(14) Zhang, H.; Zhu, G.; Jia, X.; Ding, Y.; Zhang, M.; Gao, Q.; Hu, C.; Xu, S. *J. Environ. Sci.* **2011**, *23*, 1983–1988.

(15) Semião, A. J. C.; Schäfer, A. I. *J. Membr. Sci.* **2011**, *381*, 132–141.

(16) Al-Rifai, J. H.; Khabbaz, H.; Schäfer, A. I. *Sep. Purif. Technol.* **2011**, *77*, 60–67.

(17) Geim, A. K.; Novoselov, K. S. *Nat. Mater.* **2007**, *6*, 183–191.

(18) Demirbas, A. *J. Hazard. Mater.* **2009**, *167*, 1–9.

(19) Duran, A.; Tuzen, M.; Soylak, M. *J. Hazard. Mater.* **2009**, *169*, 466–471.

(20) Yang, S.; Li, J.; Shao, D.; Hu, J.; Wang, X. *J. Hazard. Mater.* **2009**, *166*, 109–116.

(21) Ruparelia, J. P.; Duttagupta, S. P.; Chatterjee, A. K.; Mukherji, S. *Desalination* **2008**, *232*, 145–156.

(22) Zabihi, M.; Ahmadpour, A.; Asl, A. H. *J. Hazard. Mater.* **2009**, *167*, 230–236.

(23) Matsui, Y.; Fukuda, Y.; Inoue, T.; Matsushita, T. *Water Res.* **2003**, *37*, 4413–4424.

(24) Artiles, M. S.; Rout, C. S.; Fisher, T. S. *Adv. Drug Delivery Rev.* **2011**, *63*, 1352–1360.

(25) Balapanuru, J.; Yang, J.-X.; Xiao, S.; Bao, Q.; Jahan, M.; Polavarapu, L.; Wei, J.; Xu, Q.-H.; Loh, K. P. *Angew. Chem., Int. Ed.* **2010**, *49*, 6549–6553.

(26) Min, S. K.; Kim, W. Y.; Cho, Y.; Kim, K. S. *Nat. Nanotechnol.* **2011**, *6*, 162–165.

(27) Gao, W.; Majumder, M.; Alemany, L. B.; Narayanan, T. N.; Ibarra, M. A.; Pradhan, B. K.; Ajayan, P. M. *ACS Appl. Mater. Interfaces* **2011**, *3*, 1821–1826.

(28) Sreeprasad, T. S.; Maliyekkal, S. M.; Lisha, K. P.; Pradeep, T. *J. Hazard. Mater.* **2011**, *186*, 921–931.

(29) Chandra, V.; Kim, K. S. *Chem. Commun.* **2011**, *47*, 3942–3944.

(30) Chandra, V.; Park, J.; Chun, Y.; Lee, J. W.; Hwang, I.-C.; Kim, K. S. *ACS Nano* **2010**, *4*, 3979–3986.

(31) Imamoglu, M.; Tekir, O. *Desalination* **2008**, *228*, 108–113.

(32) Mishra, A. K.; Ramaprabhu, S. *Desalination* **2011**, *282*, 39–45.

(33) Zabihi, M.; Ahmadpour, A.; Asl, A. H. *J. Hazard. Mater.* **2009**, *167*, 230–236.

(34) Li, J.; Guo, S.; Zhai, Y.; Wang, E. *Electrochem. Commun.* **2009**, *11*, 1085–1088.

(35) Yang, S.; Luo, S.; Liu, C.; Wei, W. *Colloids Surf., B* **2012**, DOI: 10.1016/j.colsurfb.2012.03.007.

(36) Ayhan, D. *J. Hazard. Mater.* **2009**, *167*, 1–9.

(37) Bradder, P.; Ling, S. K.; Wang, S.; Liu, S. *J. Chem. Eng. Data* **2010**, *56*, 138–141.

(38) Wang, C.; Feng, C.; Gao, Y.; Ma, X.; Wu, Q.; Wang, Z. *Chem. Eng. J.* **2011**, *173*, 92–97.

(39) Soylak, M.; Unsal, Y. E.; Yilmaz, E.; Tuzen, M. *Food Chem. Toxicol.* **2011**, *49*, 1796–1799.

(40) Stankovich, S.; Dikin, D. A.; Dommett, G. H. B.; Kohlhaas, K. M.; Zimney, E. J.; Stach, E. A.; Piner, R. D.; Nguyen, S. T.; Ruoff, R. S. *Nature* **2006**, *442*, 282–286.

(41) Gu, H.; Yu, Y.; Liu, X.; Ni, B.; Zhou, T.; Shi, G. *Biosens. Bioelectron.* **2012**, *32*, 118–126.

(42) Maliyekkal, S. M.; Lisha, K. P.; Pradeep, T. *J. Hazard. Mater.* **2010**, *181*, 986–995.

(43) Sreeprasad, T. S.; Maliyekkal, M. S.; Deepti, K.; Chaudhari, K.; Xavier, P. L.; Pradeep, T. *ACS Appl. Mater. Interfaces* **2011**, *3*, 2643–2654.

(44) Ruan, G.; Sun, Z.; Peng, Z.; Tour, J. M. *ACS Nano* **2011**, *5*, 7601–7607.

(45) Ruiz-Hitzky, E.; Darder, M.; Fernandes, F. M.; Zatile, E.; Palomares, F. J.; Aranda, P. *Adv. Mater.* **2011**, *23*, 5250–5255.

(46) Warta, C. L.; Papadimas, S. P.; Sorial, G. A.; Suidan, M. T.; Speth, T. F. *Water Res.* **1995**, *29*, 551–562.

(47) Yu, F.; Ma, J.; Wu, Y. *J. Hazard. Mater.* **2011**, *192*, 1370–1379.

(48) Derylo-Marczewska, A.; Buczek, B.; Swiatkowski, A. *Appl. Surf. Sci.* **2011**, *257*, 9466–9472.

(49) Liu, F.; Chung, S.; Oh, G.; Seo, T. S. *ACS Appl. Mater. Interfaces* **2011**, *4*, 922–927.

(50) Annadurai, G.; Juang, R.-S.; Lee, D.-J. *J. Environ. Sci. Health, Part A* **2001**, *36*, 715–725.

(51) Lagergren, S. *K Sven Ventenskapsakad Handl* **1898**, *24*, 1–39.

(52) Yuh-Shan, H. *Scientometrics* **2004**, *59*, 171–177.

(53) Ho, Y. S.; McKay, G. *Water Res.* **2000**, *34*, 735–742.

(54) Lisha, K. P.; Maliyekkal, S. M.; Pradeep, T. *Chem. Eng. J.* **2010**, *160*, 432–439.

(55) Hutchins, R. A. *Chem. Eng. J.* **1973**, *80*, 133–138.